Biochemistry

pubs.acs.org/biochemistry Article

Cryo-EM of the Nucleosome Core Particle Bound to Ran-RCC1 Reveals a Dynamic Complex

Shuya Kate Huang,* John L. Rubinstein,* and Lewis E. Kay*

Cite This: *Biochemistry* 2024, 63, 880−892 Read Online

ACCESS | Metrics & More | Article Recommendations | Supporting Information

ABSTRACT: Ras-related nuclear protein (Ran) is a member of the Ras superfamily of small guanosine triphosphatases (GTPases) and a regulator of multiple cellular processes. In healthy cells, the GTP-bound form of Ran is concentrated at chromatin, creating a Ran•GTP gradient that provides the driving force for nucleocytoplasmic transport, mitotic spindle assembly, and nuclear envelope formation. The Ran•GTP gradient is maintained by the regulator of chromatin condensation 1 (RCC1), a guanine nucleotide exchange factor that accelerates GDP/GTP exchange in Ran. RCC1 interacts with nucleosomes, which are the fundamental repeating units of eukaryotic chromatin. Here, we present a cryo-EM analysis of a trimeric complex composed of the nucleosome core particle (NCP), RCC1, and Ran. While the contacts between RCC1 and Ran in the complex are preserved compared with a previously determined structure of RCC1-Ran, our study reveals that RCC1 and Ran interact dynamically with the NCP and undergo rocking motions on the nucleosome surface. Furthermore, the switch 1 region of Ran, which plays an important role in mediating conformational changes associated with the substitution of GDP and GTP nucleotides in Ras family members, appears to undergo disorder−order transitions and forms transient contacts with the C-terminal helix of histone H2B. Nucleotide exchange assays performed in the presence and absence of NCPs are not consistent with an active role for nucleosomes in nucleotide exchange, at least *in vitro*. Instead, the nucleosome stabilizes RCC1 and serves as a hub that concentrates RCC1 and Ran to promote efficient Ran•GDP to Ran•GTP conversion.

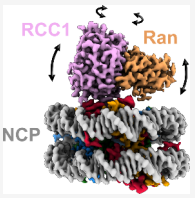

INTRODUCTION

The guanine nucleotide-binding protein Ran (Ras-related nuclear protein) is a highly conserved and abundant small GTPase that regulates multiple fundamental processes in the cell.[1,2] Ran cycles between guanosine diphosphate (GDP)-bound and guanosine triphosphate (GTP)-bound forms. During interphase, the two populations are partitioned across the nuclear envelope with Ran•GDP enriched in the cytosol and Ran•GTP in the nucleus.[3] This distribution of the two nucleotide-bound states provides a mechanism for nucleocytoplasmic transport (Figure 1A), where binding of Ran•GTP to nuclear import/export receptors facilitates shuttling of cargo across the nuclear pore complex.[4−8] During cell division, a concentration gradient of Ran•GDP/Ran•GTP is maintained following nuclear envelope breakdown, with Ran•GTP localized near chromatin.[3] This Ran•GTP gradient provides a spatial driving force for mitotic spindle assembly during cell division and nuclear envelope reformation during telophase (Figure 1B).[9−14] Disruption of the Ran•GTP gradient impairs nucleocytoplasmic transport and is associated with abnormal centrosome duplication, inhibition of antiapoptotic processes, and tumor progression.[4,15−17]

The Ran•GTP gradient is maintained by regulators of the Ran GTPase cycle. Ran GTPase activating protein 1 (RanGAP1) primarily resides in the cytoplasm and accelerates GTP hydrolysis in Ran by a factor of ∼10^5.[18−20] The only known guanine nucleotide exchange factor for Ran (RanGEF), RCC1 (regulator of chromatin condensation 1), localizes to the nucleus and accelerates GDP/GTP exchange by ∼10^5-fold as well (Figure 1A).[2,18,21,22] RCC1 is concentrated at chromatin by interacting with nucleosomes (Figure 1B), the fundamental repeating units of eukaryotic chromatin. Each nucleosome core particle (NCP) comprises approximately 147 base pairs of DNA wrapped around a scaffold of histone proteins consisting of two copies each of histone H2A, H2B, H3, and H4.[14,23,24] Nucleosome binding by RCC1 contributes to the production of Ran•GTP in the vicinity of chromatin and maintains the spatial gradient of Ran•GTP within the cell. Nucleosome binding has been reported to enhance the guanine nucleotide exchange (GEF) activity of RCC1 by ∼2-fold.[24]

On its own, Ran exhibits only modest affinity for the nucleosome, but this interaction is reinforced by the presence of RCC1.[25,26] Although structures of both Ran-RCC1 and RCC1-nucleosome complexes are known,[27,28] how NCPs, RCC1, and Ran interact to mediate nucleotide exchange is not yet understood. Further, it is unclear whether the nucleosome participates allosterically to regulate GDP release and subsequent GTP binding or simply provides a scaffold to bring RCC1 and Ran together. Here, we present structures of an NCP-RCC1-Ran complex determined by electron cryomicro-

Received: December 22, 2023
Revised: February 15, 2024
Accepted: February 29, 2024
Published: March 19, 2024

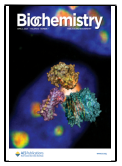

https://doi.org/10.1021/acs.biochem.3c00724
Biochemistry 2024, 63, 880−892

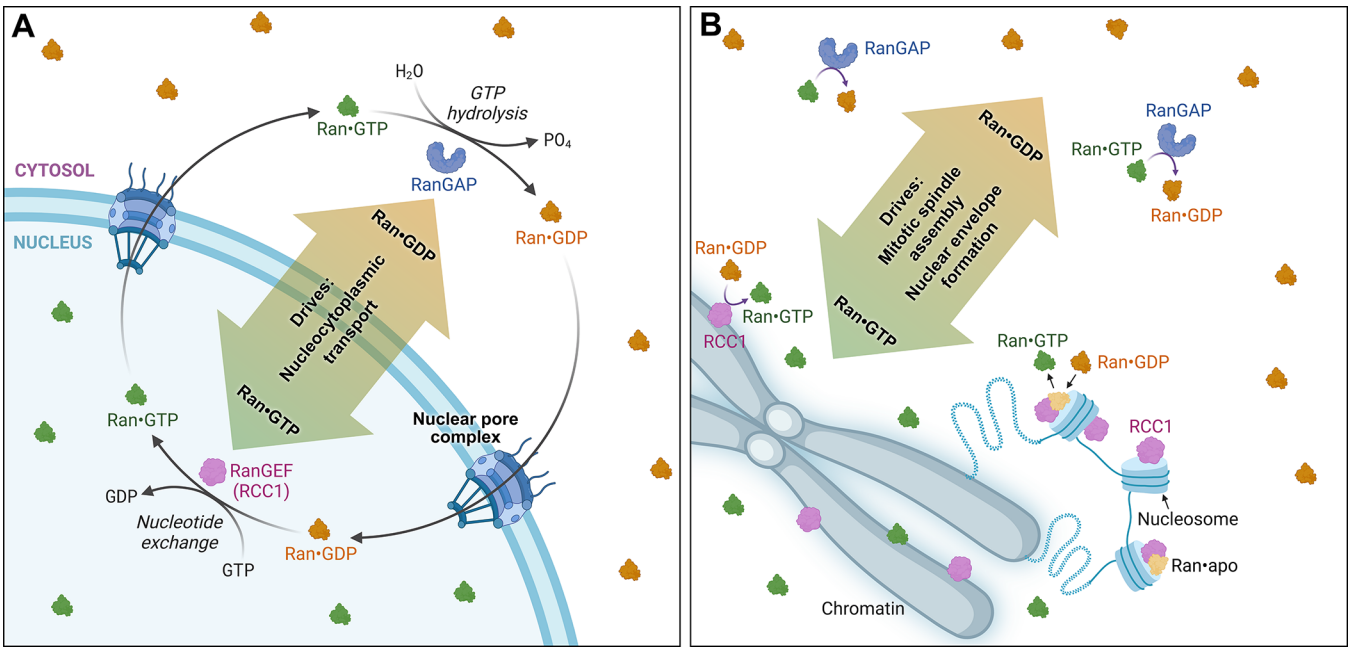

Figure 1. Ran GTPase cycle and the role of the Ran•GTP gradient in diverse cellular functions. (A) During interphase, the partition of RanGEF (RCC1) and RanGAP across the nuclear envelope gives rise to an enrichment of Ran•GTP in the nucleus and of Ran•GDP in the cytosol. This Ran•GTP gradient is important for the transport of cargo across the nuclear pore complex. (B) In the absence of a nuclear envelope (e.g., during cell division), the interaction of RCC1 with nucleosomes concentrates Ran•GTP in the vicinity of chromatin. This creates a Ran•GTP gradient as a function of distance from chromatin that facilitates mitotic spindle assembly and nuclear envelope formation.

scopy (cryo-EM). Comparisons with previous crystal structures show that the contacts between Ran and RCC1 are preserved in the ternary complex, with the position of RCC1 on the NCP shifted relative to its pose in the crystal structure. Additionally, cryo-EM shows interactions between the αC helix of histone H2B and the Ran switch 1 region, an element known to undergo conformational changes upon nucleotide exchange. Finally, fluorescent nucleotide exchange assays indicate that the nucleosome does not enhance the GEF activity of RCC1 *in vitro*, contrary to previous results.[24] Instead, the nucleosome appears to stabilize RCC1 and preserve its catalytic activity over time. Our study provides a structural model of how NCPs act as hubs to promote critical interactions between Ran and RCC1 that lead to the establishment of the Ran•GTP gradient across the cell.

MATERIALS AND METHODS

Sample Preparation. *Histones.* Histones H2A, H2B, H3, and H4 (*Drosophila melanogaster*) were expressed and purified as described previously.[29,30] A mutant H3 (C110S) was used to prevent disulfide bond formation. An isoleucine residue was inserted after the first methionine in H2B and H4 to increase the expression yield. H2A, H3, and H4 were subcloned into pET21b vectors and overexpressed without affinity tags, whereas H2B was subcloned into a pET28a vector and contained a hexahistidine tag followed by a TEV cleavage site at the N terminus. Histone plasmids were used to transform BL21-(DE3)-RIPL-CodonPlus *Escherichia coli* (*E. coli*), and cells were grown in LB media at 37 °C until reaching an OD_{600} of 0.6−0.8. Histone expression was induced with 1 mM IPTG, and cells were grown at 37 °C overnight (H2A, H2B, H3) or for 5 h (H4) before harvesting.

To purify untagged histones (H2A, H3, H4) from inclusion bodies, cell pellets were resuspended in lysis buffer (50 mM Tris-HCl, pH 7.5, 100 mM NaCl, 1% (v/v) Triton X-100) and lysed by sonication (2 s on and 2 s off for 10 min, 30% power level) on ice. The lysate was centrifuged for 30 min at 14,000*g*. The pellet was collected and resuspended in lysis buffer without Triton X-100, and the sample centrifuged again for 30 min at 14,000*g*. The pellet was resuspended in unfolding buffer (20 mM Tris-HCl, pH 7.5, 6 M GdnHCl) and incubated for 30 min until the inclusion bodies were dissolved. The sample was centrifuged to remove insoluble debris, and the supernatant was dialyzed against urea buffer (50 mM sodium phosphate, pH 7.4, 50 mM NaCl, 1 mM EDTA, 7 M urea), which was pretreated with 25 g/L Amberlite beads for 1 h at room temperature to prevent lysine carbamoylation. Dialyzed histones were purified on a 5 mL HiTrap SP XL cation exchange column (Cytiva) over a 50−1000 mM NaCl gradient. Purified histone fractions were dialyzed against Milli-Q water, lyophilized, and stored at −20 °C.

H2B cell pellets were lysed, and inclusion bodies were collected as above. The inclusion bodies were dissolved in denaturing buffer (20 mM sodium phosphate, pH 7.5, 500 mM NaCl, 20 mM imidazole, 6 M GdnHCl). Each sample was centrifuged to remove insoluble debris, and the supernatant was applied to Ni-NTA resin (Cytiva) pre-equilibrated with denaturing buffer. The resin was washed with 10 column volumes of denaturing buffer, and His-tagged H2B was eluted with elution buffer (20 mM sodium phosphate at pH 7.5, 500 mM NaCl, 300 mM imidazole, 6 M GdnHCl). The sample was buffer-exchanged to TEV cleavage buffer (20 mM sodium phosphate, pH 7.5, 500 mM Arg-HCl, 500 mM NaCl, 30 mM imidazole, 2 mM DTT) and incubated with TEV protease at room temperature for 16 h. The cleaved H2B was purified with a Ni-NTA column by collecting the flow-through, followed by dialysis against Milli-Q water, lyophilization, and storage at −20 °C.

https://doi.org/10.1021/acs.biochem.3c00724
Biochemistry 2024, 63, 880−892

601 DNA. Widom 601 DNA was produced as previously described.[29,30] Briefly, *E. coli* (Mach1) cells were transformed with pUC19 plasmids carrying 153-bp 601 DNA (~30 copies per plasmid separated by a 12-bp linker and EcoRV cleavage sites) and grown at 37 °C overnight on LB-agar plates supplemented with 100 μg/mL ampicillin. A single colony was transferred to 5 mL of Terrific Broth (Wisent Bioproducts) and grown at 37 °C to an OD_{600} of ~2.0. This 5 mL culture was transferred to 100 mL of Terrific Broth and grown at 37 °C until an OD_{600} of ~1.5. The 100 mL culture was transferred to 1 L of Terrific Broth supplemented with 100 μg/mL ampicillin, 4 mL/L glycerol, and 7 mM $MgSO_4$. This 1 L culture was grown at 37 °C overnight before harvesting. Plasmid DNA was extracted from the cell pellet with a Plasmid Gigaprep kit (QIAGEN). The purified plasmid DNA was digested with EcoRV (NEB), and the digested DNA was purified with a 5 mL HiTrap DEAE Sepharose FF column (Cytiva) over a 0−1000 mM NaCl gradient. The eluted 153-bp 601 DNA fractions were pooled and further purified on a Superdex 200 HiLoad 26/600 column pre-equilibrated in RB-high buffer (20 mM Tris-HCl, pH 7.5, 2 M KCl, 1 mM EDTA). The purified 601 DNA was concentrated to ~50 mM and stored at 4 °C.

Nucleosome Core Particles (NCPs). To reconstitute histone octamers, lyophilized H2A, H2B, H3, and H4 were dissolved in unfolding buffer (10 mM Tris-HCl, pH 7.5, 6 M GdnHCl) and combined in a 1.1:1.1:1:1 ratio at concentrations of 60−70 μM for each histone. The sample was dialyzed against refolding buffer RB-high (10 mM Tris-HCl, pH 7.5, 2 M KCl, 1 mM EDTA) overnight at 4 °C, with fresh refolding buffer added continuously to the dialysis chamber at ~1.5 mL/min while buffer flowed out through a hole at the side of the chamber. After dialysis, the sample was purified on a Superdex 200 Increase 10/300 GL column (Cytiva) equilibrated with RB-high buffer. The octamer fractions were pooled and concentrated to ~10−50 μM before reconstituting NCPs.

Histone octamer and 153-bp 601 DNA were combined in RB-high buffer at an equimolar ratio to a final concentration of 6 μM each. The sample was dialyzed over a continuous salt gradient from the RB-high buffer (400 mL) to an RB low buffer (20 mM Tris-HCl, pH 7.5, 100 mM KCl) at 4 °C for 18 h. To produce this gradient, RB low buffer was added to the dialysis chamber at ~1.5 mL/min, while the buffer in the chamber flowed out through a hole at the side of the chamber. The reconstituted NCPs were stored at 4 °C or buffer-exchanged for downstream applications.

Ran. A pET28a vector carrying the gene encoding full-length human Ran immediately downstream of an open reading frame for an N-terminal His_6-SUMO tag was purchased from GenScript. The plasmid was used to transform BL21 (DE3) *E. coli* cells, and a single colony of the transformant was grown in 20 mL of LB media with 50 μg/mL kanamycin at 37 °C overnight. This preculture was used to inoculate 1 L of LB media supplemented with 50 μg/mL kanamycin. The cells were grown at 37 °C until an OD_{600} of ~0.6, and protein expression was induced with 0.25 mM IPTG overnight at 25 °C. Cells were harvested, resuspended in lysis buffer (20 mM Tris-HCl, pH 7.5, 300 mM KCl, 2 mM $MgCl_2$, 20 mM imidazole, 10% (v/v) glycerol, 1 mM TCEP, 0.5 mg/mL lysozyme, 5 μg/mL DNase, 10 μM GDP), and lysed by sonication. The lysate was centrifuged at 14,000*g* for 90 min, and the supernatant was loaded onto a Ni-NTA column equilibrated with lysis buffer. The column was washed with 5 column volumes of wash buffer (20 mM Tris-HCl, pH 7.5, 300 mM KCl, 2 mM $MgCl_2$, 20 mM imidazole, 10% (v/v) glycerol, 1 mM TCEP, 10 μM GDP), and His_6-SUMO-Ran was eluted with elution buffer (20 mM Tris-HCl, pH 7.5, 100 mM KCl, 2 mM $MgCl_2$, 250 mM imidazole, 1 mM TCEP, 10% (v/v) glycerol, 10 μM GDP). The eluted protein was buffer-exchanged to SUMO cleavage buffer (20 mM Tris-HCl at pH 7.5, 100 mM KCl, 2 mM $MgCl_2$, 1 mM TCEP, 10% (v/v) glycerol, 10 μM GDP) and incubated with Ulp1 at 4 °C overnight. Untagged Ran was purified with a Ni-NTA column by collecting the flow-through. The sample was further purified with a Superdex 75 16/600 size exclusion column (Cytiva) equilibrated with storage buffer (20 mM Tris-HCl at pH 7.5, 100 mM KCl, 2 mM $MgCl_2$, 1 mM TCEP, 10% (v/v) glycerol). The purified Ran was aliquoted, flash-frozen with liquid nitrogen, and stored at −80 °C until use.

RCC1. A pET28a vector carrying the gene encoding full-length human RCC1 (residues 2-421, α isoform) immediately downstream of an open reading frame for an N-terminal His_6-SUMO tag was purchased from GenScript. The plasmid was used to transform BL21 (DE3) *E. coli* cells, and a single colony of the transformant was grown in 20 mL of LB media supplemented with 50 μg/mL kanamycin at 37 °C overnight. The preculture was transferred to 1 L of LB media supplemented with 50 μg/mL kanamycin, and the cells were grown at 37 °C until reaching an OD_{600} of ~0.6. Expression of RCC1 was induced with 0.5 mM IPTG for 4 h at 37 °C prior to harvesting by centrifugation. Cells were resuspended in lysis buffer (20 mM Tris-HCl, pH 8.0, 300 mM KCl, 2 mM $MgCl_2$, 30 mM imidazole, 10% (v/v) glycerol, 1 mM TCEP, 0.5 mg/mL lysozyme, and 10 μg/mL DNase) and lysed by sonication. The lysate was centrifuged at 14,000*g* for 90 min, and the supernatant was loaded onto a Ni-NTA column equilibrated with lysis buffer. The resin was washed with 5 column volumes of wash buffer (20 mM Tris-HCl, pH 8.0, 300 mM KCl, 2 mM $MgCl_2$, 30 mM imidazole, 10% (v/v) glycerol, 1 mM TCEP), and His_6-SUMO-RCC1 was eluted with elution buffer (20 mM Tris-HCl, pH 8.0, 300 mM KCl, 250 mM imidazole, 1 mM TCEP, 10% (v/v) glycerol). The eluted sample was incubated with Ulp1 at 4 °C overnight while dialyzing against Ulp1 buffer (20 mM Tris-HCl, pH 8.0, 300 mM KCl, 1 mM TCEP, 10% (v/v) glycerol). Untagged RCC1 was purified on a 5 mL HisTrap HP column (Cytiva) over a 0−250 mM imidazole gradient. RCC1 eluted at ~50 mM imidazole. The sample was further purified with a Superdex 75 16/600 size exclusion column equilibrated with storage buffer (20 mM Tris-HCl (pH, 8.0), 150 mM KCl, 1 mM TCEP, 10% (v/v) glycerol). The purified RCC1 was aliquoted, flash-frozen with liquid nitrogen, and stored at −80 °C until use.

Cryo-EM Sample Preparation and Data Collection. Proteins were combined to a final concentration of 0.8 μM NCP, 5 μM RCC1, 7.5 μM Ran, and 1 U/mL apyrase in complexation buffer (20 mM Tris-HCl (pH 7.5) and 50 mM KCl, 2 mM $MgCl_2$, 1 mM TCEP, and 0.875 mM EDTA). The sample was incubated for 1 h prior to grid freezing. Holey gold grids were prepared in-house[31] and glow-discharged in air for 30 s immediately prior to sample application. The sample (3 μL) was applied to each grid, followed by blotting from the holey-film side at 4 °C and ~95% humidity with a Leica EM GP2 plunge freezer (Leica Microsystems) for ~2 s (0 s in the Leica setting). Grids were plunge-frozen in liquid ethane. The sample was imaged with a Titan Krios G3 electron microscope (ThermoFisher Scientific) operating at 300 kV and with a nominal magnification of 75,000×, corresponding to a calibrated pixel size of 1.03 Å. Data were collected with a Falcon 4i camera (ThermoFisher Scientific) and automated with the EPU

https://doi.org/10.1021/acs.biochem.3c00724
Biochemistry 2024, 63, 880−892

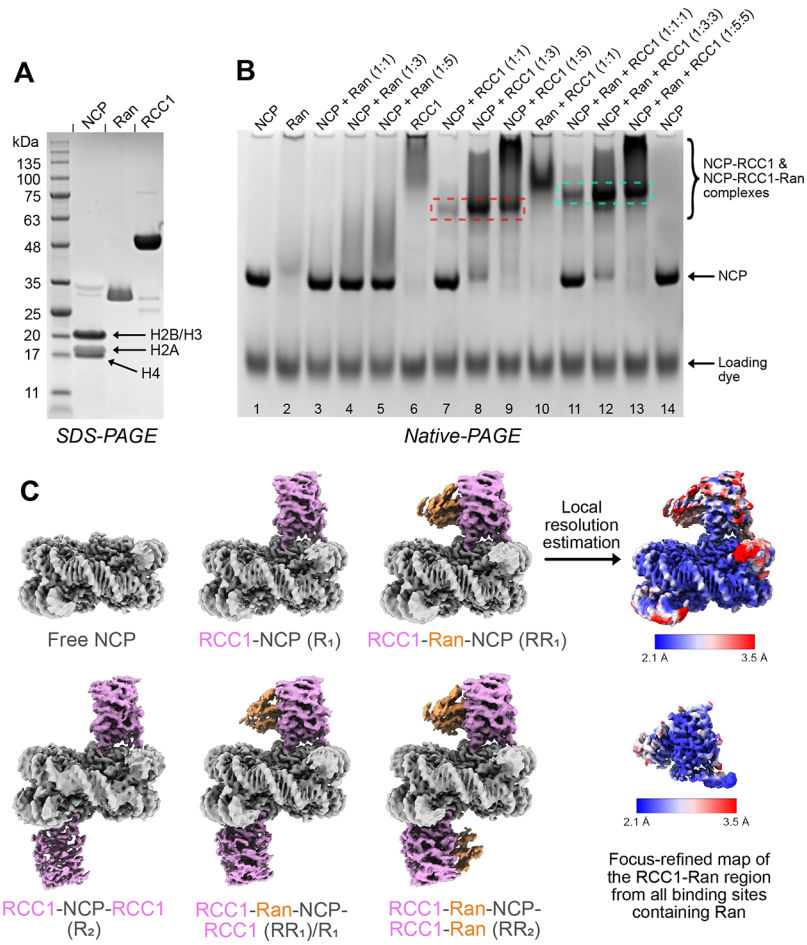

Figure 2. Purified NCP, RCC1, and Ran form complexes with variable binding stoichiometries. (A) SDS-PAGE gel of purified NCP, Ran, and RCC1. (B) Native-PAGE gel of NCP (lanes 1 and 14), Ran•GDP (lane 2), NCP + Ran•GDP (lanes 3−5), RCC1 (lane 6), NCP + RCC1 (lanes 7−9), Ran•apo + RCC1 (lane 10), and NCP + Ran•apo + RCC1 (lanes 11−13) in various stoichiometric ratios. The NCP band is shifted in the presence of either RCC1 (red dotted box) or RCC1 + Ran (cyan dotted box). In lanes 10−13, 1 U/mL apyrase was added to remove copurified GDP from Ran•GDP, producing Ran•apo. The diffuse and poorly stained bands for Ran (lane 2) and RCC1 (lane 6) alone may result from the low acrylamide concentration (7%) used, leading to increased diffusion for Ran (~24 kDa) and RCC1 (~45 kDa) relative to NCPs (~200 kDa) and, therefore, smearing of bands. Additionally, the isoelectric points for Ran and RCC1 are close to neutral, resulting in less electrophoresis-induced band migration compared to charged particles. Finally, band diffusion could be a result of conformational heterogeneity, which may arise from Ran's C-terminal tail and RCC1's N-terminal tail, both of which are about 40-residues long and flexible. (C) Unsharpened cryo-EM maps of free NCP, NCP-RCC1 complexes, and NCP-RCC1-Ran complexes from a single data set. Local resolution for a map of NCP with RCC1-Ran bound on one side (upper) is shown, along with local resolution for a map of RCC1-Ran from focused refinement.

software (ThermoFisher Scientific) while applying a defocus range of 1.0−2.0 μm. 6973 movies were acquired with 40 exposure fractions per movie, at an exposure rate of ~6.1 e^-/pixel/s and a total exposure of ~42 $e^-/Å^2$.

Cryo-EM Data Processing. The image processing pipeline is summarized in Figure S1. Except for local sharpening, all image analysis steps were carried out with cryoSPARC v.4.[32] Patch-based motion correction and contrast transfer function (CTF) parameter estimation were performed in cryoSPARC Live. Particles in micrographs were selected with templates generated from a previous NCP map, yielding 1,572,329 particle images. The particle image stack was cleaned with several rounds of 2D classification and *ab initio* reconstruction followed by heterogeneous refinement to eliminate low-quality images and most images of free NCPs. The remaining 481,661 particle images consist of a small number of images of free NCPs and images of NCPs bound to RCC1 or RCC1 + Ran on either one or both faces of the NCP.

Note that the NCP carrying a nonpalindromic 601 DNA sequence is characterized by C2 pseudo symmetry. To systematically separate different binding states, an initial map was obtained from non-uniform refinement[33] using all 481,661 particle images while applying C2 symmetry. This procedure was followed by focused 3D classification with a mask over the Ran and RCC1 binding region on one side (the "top") of the nucleosome to yield three distinct classes: no protein bound, RCC1 + Ran bound, and RCC1 bound without Ran. Each of these three classes was subjected to another round of focused 3D classification with a mask over the Ran and RCC1 binding region on the other side (the "bottom") of the NCP to once again yield three different classes corresponding to no protein bound in this region, RCC1 + Ran bound, and RCC1 bound without Ran.

The nine classes from above were sorted and grouped accordingly (Figure S1) to give six different binding states while ignoring DNA sequence asymmetry: free NCPs, RCC1 bound on one side (R_1), RCC1 bound on both sides (R_2), RCC1 + Ran

https://doi.org/10.1021/acs.biochem.3c00724
Biochemistry 2024, 63, 880−892

bound on one side ($(RR)_1$), RCC1 + Ran bound on both sides ($(RR)_2$), and RCC1 + Ran bound on one side with RCC1 bound on the other side ($(RR)_1/R_1$). Non-uniform refinement was carried out to calculate a map for each of the six classes. In all six maps, NCP appeared to be better resolved than RCC1 and Ran. To produce a map with improved resolution of the RCC1/Ran binding region, particle images from the latter three classes with RCC1 + Ran bound were pooled (Figure S1), subjected to reference-based motion correction and exposure weighting, and used as input for non-uniform refinement applying C2 symmetry. This refinement was followed by symmetry expansion around the C2 axis, yielding 772,724 particle images. A final round of focused 3D classification over one of the binding sites (top) resulted in 401,603 particle images containing both RCC1 and Ran. A final map of RCC1 and Ran from the top binding site was refined with these particle images. To make a composite map containing high-resolution NCP (from the $(RR)_1$ map) and RCC1-Ran (from the locally refined RCC1-Ran map), local sharpening was performed for each map using *LocalDeblur* implemented in Scipion.[34,35] The two maps were then combined in UCSF ChimeraX[36] to generate the composite map for atomic model building. Data processing statistics are summarized in Table S1. Three-dimensional variability analysis (3DVA) was carried out on the focus-refined data set with a mask around either RCC1-Ran or RCC1.

Model Building and Refinement. A previously published NCP model (PDB:1KX5)[37] and the AlphaFold models of RCC1 and Ran[38] were fitted into the NCP-RCC1-Ran composite map with UCSF ChimeraX.[36] Atomic models were constructed by iterative manual model building in Coot[39] followed by real space refinement with ISOLDE and Phenix.[40,41] The nonpalindromic DNA sequence and application of pseudo C2 symmetry resulted in incoherent averaging of the density from each nucleotide base with the pseudosymmetry-related base. This averaging produced poorly resolved densities for many base pairs. Nonetheless, using the known sequence of the DNA, a model was built that fits the map reasonably well. Figures were rendered with UCSF ChimeraX.[36] Model building statistics are summarized in Table S1.

Native-PAGE. The following samples (corresponding to the native-PAGE gel lanes 1−14 in Figure 2) were prepared at the indicated final concentration in Ran storage buffer (20 mM Tris-HCl at pH 7.5, 100 mM KCl, 2 mM $MgCl_2$, 1 mM TECP):

1. 1 μM NCP
2. 5 μM Ran•GDP
3. 1 μM NCP + 1 μM Ran•GDP
4. 1 μM NCP + 3 μM Ran•GDP
5. 1 μM NCP + 5 μM Ran•GDP
6. 5 μM RCC1
7. 1 μM NCP + 1 μM RCC1
8. 1 μM NCP + 3 μM RCC1
9. 1 μM NCP + 5 μM RCC1
10. 5 μM Ran•GDP + 5 μM RCC1 + 1 U/mL apyrase
11. 1 μM NCP + 1 μM Ran•GDP + 1 μM RCC1 + 1 U/mL apyrase
12. 1 μM NCP + 3 μM Ran•GDP + 3 μM RCC1 + 1 U/mL apyrase
13. 1 μM NCP + 5 μM Ran•GDP + 5 μM RCC1 + 1 U/mL apyrase
14. 1 μM NCP

The samples were incubated for 30 min prior to the addition of FastDigest Green Buffer to a final 1× working concentration (Thermo Fisher Scientific) and loading onto a 7% polyacrylamide gel. The gel was run for 60 min at 150 V, with the electrophoresis cassette on ice using a 1× Tris-borate EDTA running buffer. The gel was stained with Coomassie Brilliant Blue R-250 stain for 30 min prior to destaining and imaging.

Fluorescent Nucleotide Exchange Assays. 2′/3′-*O*-(*N*-Methyl-anthraniloyl)-GDP (MANT-GDP)-loaded Ran was produced by incubating purified Ran•GDP with a 30-fold excess of MANT-GDP (Jena Bioscience) at room temperature for 6 h. Exchange of GDP for MANT-GDP was carried out in 20 mM Tris-HCl, pH 7.5, 100 mM KCl, 1 mM TECP, 10 mM EDTA. Excess nucleotide was removed by gel filtration with a Superdex 75 10/300 column (Cytiva) equilibrated with Ran storage buffer (20 mM Tris-HCl, pH 7.5, 100 mM KCl, 2 mM $MgCl_2$, 1 mM TECP). MANT-GDP loading was confirmed by monitoring the increase in fluorescence resonance energy transfer of Ran's intrinsic tryptophan fluorescence (λ_{ex} = 280 nm, λ_{em} ~330 nm) to the MANT group of the bound MANT-GDP (λ_{em} ~450 nm).

Nucleotide exchange reactions were monitored with a BioTek Synergy Neo2 multimode microplate reader using a 384-well black plate with 0.7 μM Ran-MANT-GDP in Ran storage buffer and a reaction volume of 20 μL. Fluorescence measurements were performed at room temperature in 10 s intervals for a total of 45 min with λ_{ex} = 355 nm, λ_{em} = 448 nm, and a 15 nm bandpass. Nucleotide exchange was initiated by adding unlabeled GDP to a final concentration of 100 μM with or without 3 nM RCC1, which was preincubated in buffer with or without NCP for 0, 8, 16, 24, 32, or 40 min prior to injection.

Least-squares linear regression was done with GraphPad Prism 8.4.2, using the initial 100 s of the MANT-GDP dissociation curves while treating each replicate value as an individual point. Relative nucleotide exchange rates were calculated by taking the ratio of the slope for each fitted line and the slope of the fitted line in the absence of RCC1 and NCP.

RESULTS AND DISCUSSION

Cryo-EM of NCP-RCC1-Ran Complexes. To facilitate structure determination of the NCP-RCC1-Ran complex (Figure S1), we produced recombinant full-length human RCC1 (α-isoform) and human Ran (purified in the form of Ran•GDP), as well as NCPs reconstituted using a 153-bp Widom 601 DNA sequence[42] and histones from *Drosophila melanogaster* (Figure 2A). Histones are extremely well conserved among different organisms[43] with 95, 96, 99, and 100% sequence identities between the core H2A, H2B, H3, and H4 domains of human and *Drosophila* histones. Less identity is found in a comparison of the histone tail regions. Notably, our structural work establishes that there is no difference in sequence between human and *Drosophila* histones at regions near or contacting Ran/RCC1 (see below). Any effects from the substitution of *Drosophila* histones for their human counterparts in this study are thus expected to be minimal. The purified proteins mentioned above were combined in various stoichiometric ratios and tested for their ability to form complexes using native polyacrylamide gel electrophoresis (native-PAGE) (Figure 2B). The NCPs migrated as a single band (lane 1) that was gel-shifted upon the addition of RCC1 (lanes 7−9), indicating complex formation. Although direct binding between NCP and Ran has been reported previously,[26] we observed little gel shift when NCP was mixed with Ran alone (lanes 3−5), suggesting that, under our conditions, NCP and Ran interact weakly, if at all. In contrast, Ran and RCC1 appear to form a

https://doi.org/10.1021/acs.biochem.3c00724
Biochemistry 2024, 63, 880−892

stoichiometric complex when combined in a 1:1 ratio (lane 10). We also observed the formation of NCP-RCC1-Ran complexes when all three species were combined, as evident from the appearance of a band at higher molecular weight on the gel compared to the main NCP-RCC1 band (lanes 11−13). Note that, in samples containing both Ran and RCC1, apyrase was added to remove copurified GDP from Ran because GEF binding affinities to GTPases are generally reduced in the presence of nucleotide.[44,45] The results from native-PAGE suggest that NCP, Ran, and RCC1 form a complex *in vitro* mediated by interactions between NCP and RCC1 and between RCC1 and Ran. The binding of RCC1 or RCC1 + Ran to NCP required an excess of RCC1 or RCC1 + Ran to achieve a complete gel shift of the NCP band, suggesting that these species do not interact with NCP with a high affinity.

To encourage complex formation, we used a ∼1:6:9 ratio of NCP:RCC1:Ran for cryo-EM studies and treated the sample with apyrase for 1 h prior to grid freezing. The resulting micrographs and 2D class averages show free NCPs as well as NCPs bound to RCC1 and to both RCC1 and Ran (Figure S2A). Particle selection for NCPs, followed by rounds of 2D and 3D classification, uncovered multiple binding states, including free NCPs, NCP-RCC1 complexes, and NCP-RCC1-Ran complexes where RCC1 and RCC1 + Ran are bound to one or both faces of the NCP. For free NCPs and two-side binding states where the top and bottom faces of the NCP are complexed either with RCC1 or RCC1 + Ran, pseudo C2 symmetry is observed. This property allowed enforcement of C2 symmetry during early stages of data processing to systematically classify the data set leading to maps of six major binding states: free NCPs, RCC1 bound on one side (R_1), RCC1 bound on both sides (R_2), RCC1 + Ran bound on one side ($(RR)_1$), RCC1 + Ran bound on both sides ($(RR)_2$), and RCC1 + Ran bound on one side with only RCC1 bound on the other side ($(RR)_1/R_1$) (Figure 2C and Figure S1). NCP-Ran complexes were not detected in the absence of RCC1, consistent with the observation from native-PAGE and previous cross-linking mass spectrometry that Ran interacts with the nucleosome *in vitro* only in the presence of RCC1.[25]

While the NCP portion of several maps refined to better than 3 Å resolution, the resolution of the RCC1-Ran portion remained poor in each of the individual maps owing to the flexibility of these components on the surface of the nucleosome (see below), as illustrated by a map of local resolution in the structure of the complex (Figure 2C). To improve the RCC1-Ran region of the map, particle images from all classes containing Ran ($(RR)_1$, $(RR)_2$, and $(RR)_1/R_1$) were combined, symmetry-expanded, and subjected to focused classification isolating all particles with Ran density (Figure S1). Local refinement of an RCC1-Ran map with this final stack of 401,603 particle images gave an overall nominal resolution of 2.5 Å. The RCC1-Ran map from local refinement was combined with the NCP portion of the $(RR)_1$ map (overall nominal resolution of 2.4 Å) to produce a composite map for model building and further analysis (Figure S1).

Overall Structure of the NCP-RCC1-Ran Complex. The overall architecture of the NCP-RCC1-Ran complex is consistent with the previously predicted topology for the assembly, based on structures of the individual components and pairs of components.[25,28,46] Both RCC1 and Ran are positioned on the nucleosome surface, with the beta propeller of RCC1 binding on its side to the folded region of histones H2A/H2B and the beta-wedge face of the propeller interacting with Ran (Figure 3A,B). The binding of RCC1 to the NCP is mostly mediated through electrostatic interactions between the

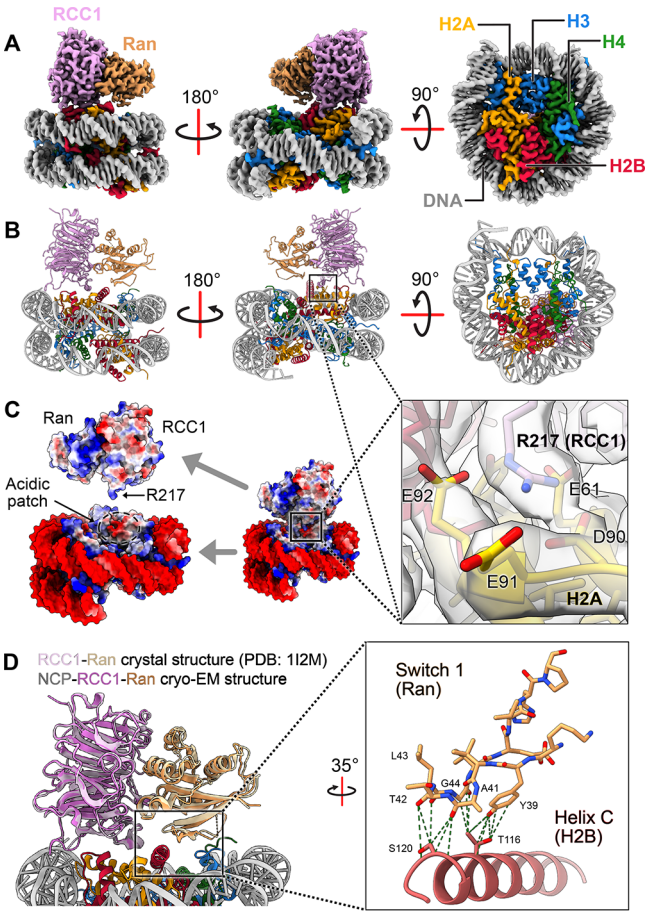

Figure 3. Cryo-EM structure of the NCP-RCC1-Ran complex. (A) Composite map of the NCP-RCC1-Ran complex and its corresponding atomic model (B) with RCC1 colored in plum, Ran in dark orange, H2A in yellow, H2B in red, H3 in blue, H4 in green, and DNA in gray. (C) Surface representation of the NCP-RCC1-Ran complex colored by the electrostatic potential. The RCC1-Ran and NCP portions are separated vertically on the left to highlight the acidic patch in the NCP and the anchoring residue R217 in RCC1. Inset on the right shows a close-up view of R217 interacting with the acidic patch with cryo-EM densities and fitted atomic models. (D) Overlay of the RCC1-Ran atomic model from X-ray crystallography (PDB: 1I2M) and the atomic model of NCP-RCC1-Ran from cryo-EM. Inset shows a blow-up of the cryo-EM model for the switch 1 region of Ran and the C-terminal helix of H2B. Potential interacting residues are labeled, and pairs of nonhydrogen atoms with interatomic distances of <5 Å are indicated with green dashed lines.

arginine anchor R217 of RCC1 and the acidic patch residues in H2A (Figure 3C). While the histone core of the NCP is predominantly positively charged, the H2A/H2B acidic patch serves as a common binding site for histone modifying enzymes and chromatin factors, including Dot1L, COMPASS, RNF168, PRC1, SET8, HMGN2, and RCC1.[47,48] Residue R217 in RCC1 is conserved across species, with the R217A mutant significantly reducing its ability to bind nucleosomes.[46] In the NCP-RCC1-Ran complex, R217 inserts into the primary groove of the acidic patch to form an electrostatic attachment between RCC1 and the NCP.

https://doi.org/10.1021/acs.biochem.3c00724
Biochemistry 2024, 63, 880−892

The RCC1-Ran portion of the assembly is nearly identical to a previous crystal structure of RCC1-Ran•apo in the absence of the NCP[27] (Figure 3D). The RCC1-Ran binding interface is preserved, and both structures of Ran feature an unresolved C-terminal tail. In contrast, previous Ran•GDP and Ran•GTP-RanGAP1-RanBP1 crystal structures show the C-terminal tail adopting distinct conformations, for instance forming a helix that either packs against Ran's protein core (in Ran•GDP) or wraps around RanBP1 (in Ran•GTP-RanGAP1-RanBP1).[49,50] The only interaction between Ran and the nucleosome in the present cryo-EM map involves part of Ran's switch 1 region and the C-terminal helix of histone H2B. Like other GTPases, the switch regions from Ran are known to undergo conformational changes upon binding different nucleotides and effectors. For example, in the Ran•GDP crystal structure, switch 1 adopts a conformation that comprises a short helix (residues L31-E36) followed by a beta hairpin motif (residues K37-V45).[49,51] The helix region is disordered in the RCC1-Ran•apo crystal structure, and the entire switch 1 is disordered in the Ran•GTP-RanGAP1-RanBP1 structure.[27,50] In the structure of the NCP-RCC1-Ran complex presented here, the beta hairpin portion of switch 1 contacts the C-terminal helix of H2B. However, this hairpin element appears flexible, as it exhibits local resolution that is worse than the rest of Ran (Figure 3D, Figures S2 and S4, and the Supporting Information, Movie 3).

To explore underlying dynamics that may be present in the complex, we employed the 3D variability analysis (3DVA) tool in cryoSPARC, performing the analysis within a mask that included the RCC1-Ran region of the map.[32,52] 3DVA uses principal component analysis (PCA) to explore heterogeneity in the data set and reconstructs families of 3D volumes with each member of the family consisting of the consensus map with addition or subtraction of density from the map. Components from PCA can correspond to movement in the map or dissociation of a subunit. Each family of 3D volumes can represent a "reaction coordinate" that describes variability in the particle images used to construct the consensus map with the largest component of variability described by the first principal component (component 0). Results from 3DVA are presented in Supplementary Movies 1−3, and the first and last frames from each of the first three principal component movies are shown in Figure 4. The first two components show Ran and RCC1 rocking back and forth as a unit either parallel (component 0) or perpendicular (component 1) to the plane of the nucleosome. The third variability component (component 2) captures the motion of Ran's switch 1 region, which appears to undergo a disorder-to-order transition upon interaction with the αC helix of H2B. The functional consequence of this interaction is unclear. However, it is possible that the interaction of Ran with the nucleosome plays a role in regulating nucleotide exchange or facilitating the retention of Ran at the nucleosome surface (see below).

Despite the lack of extensive Ran-NCP contacts in our structure, previous studies reported single-micromolar binding affinities between the nucleosome and Ran•GDP/Ran•GTP.[26] An *in vitro* cross-linking mass spectrometry study using a Ran-E70A mutant with reduced ability to release GDP found cross-links between Ran and histone H4 in the presence of RCC1.[25] In intact nuclei from human osteosarcoma U2OS cells, Ran was cross-linked to histones H2B, H3, and H4.[25] Additionally, Ran•GTP was found to form a complex with H2A-H2B and the histone chaperone importin 9 (as well as its yeast homologue Kap114) during nucleosome assembly.[53,54] In these ternary

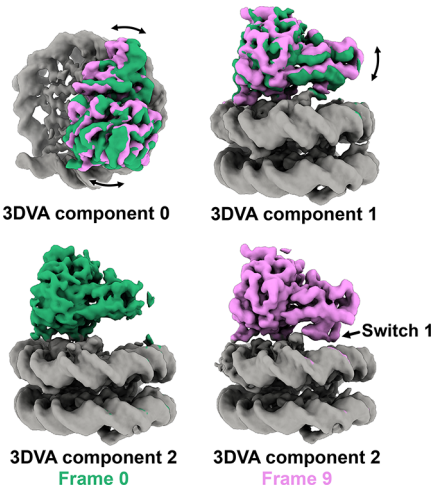

Figure 4. 3D variability analysis of the RCC1-Ran region in the NCP-RCC1-Ran complex. Results from the first three principal components are shown, where the first and last frames from each movie (Supplementary Movies 1−3) are colored green and pink, respectively. For components 0 and 1, curved arrows highlight the primary motion detected in each component.

complexes, Ran•GTP modulates importin-histone interactions and makes transient contacts with α3 and αC of H2A. The complexation leads to a conformational change in importin 9/Kap114 that promotes the release of H2A-H2B into the assembling nucleosome. As importin-9 binds to H2A-H2B via a mechanism also involving arginine interactions with the acidic patch as well as to Ran,[53,54] it is conceivable that, in the vicinity of chromatin, a high concentration of RCC1 may result in competition between importins and RCC1 for binding to both H2A-H2B and Ran. The Ran-nucleosome interactions mentioned above are not observed in our structure, which features Ran in its (mostly) nucleotide-free state (see below). It is possible that nucleotide-free Ran, while binding more tightly to RCC1, has a reduced affinity for the NCP. Furthermore, transient interactions that might occur between flexible elements in Ran and the nucleosome would not be resolved in the cryo-EM map.

Dynamic RCC1 Interactions with the NCP. The position of RCC1 on the nucleosome surface is rotated in cryo-EM-determined NCP-RCC1 and NCP-RCC1-Ran complex structures relative to its pose in a previously determined crystal structure of *Drosophila* RCC1 bound to the NCP[28] (Figure 5A, compare gold and gray structures). In the crystal structure, RCC1 is found on both faces of the nucleosome, with a long loop within its beta propeller structure, named the switchback loop, binding to the H2A/H2B acidic patch on the NCP surface through residues R223 and R216. These interactions are preserved in the cryo-EM structure presented here, which features R217 (equivalent to R223 in *Drosophila* RCC1) as the major arginine anchor (Figures 3C and 5A). Interestingly, between the two structures, RCC1 is rotated by ∼32° about an axis that passes through R217 (Figure 5B). The switchback loop also serves as a pivot for the motion observed in component 0 of the 3D variability analysis above, where RCC1-Ran rotates as a unit parallel to the plane of the nucleosome. The different binding pose between the crystal and cryo-EM structures could simply be a result of crystal packing (X-ray) or air−water interface (cryo-EM) effects or, alternatively, may arise from inherent differences between human and *Drosophila* RCC1

https://doi.org/10.1021/acs.biochem.3c00724
Biochemistry 2024, 63, 880−892

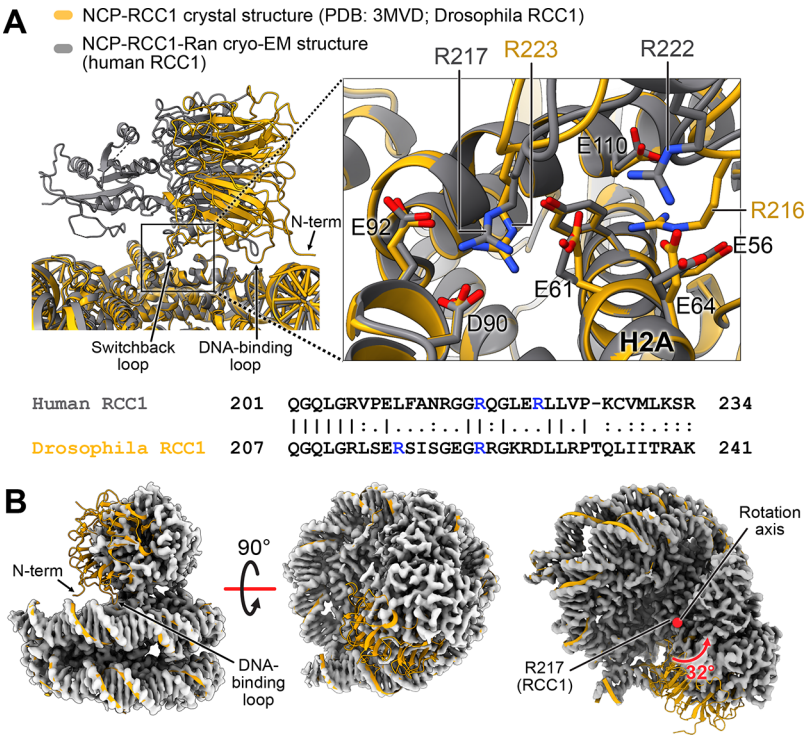

Figure 5. Dynamic NCP-RCC1 interaction. (A) Overlay of the atomic model of NCP-RCC1-Ran from cryo-EM (gray) and NCP-RCC1 from X-ray crystallography (yellow, PDB: 3MVD) with the NCP portions aligned. The resolved portion of the RCC1 N-terminal tail and DNA-binding loop are indicated with arrows for the crystal structure. Inset shows a close-up view of key arginine residues in the RCC1 switchback loop and the acidic patch residues in the NCP. The arginine residues shown are highlighted in the human and *Drosophila* RCC1 sequence alignment in blue. (B) The NCP-RCC1-Ran cryo-EM map (gray) with the NCP region of the NCP-RCC1 X-ray crystal structure (yellow, PDB: 3MVD) fitted in the map. The change in RCC1 binding pose between the two structures can be described as a 32° rotation around an axis that passes through residue R217 of RCC1 (shown as a red dot representing a rotation axis perpendicular to the plane of the page).

variants, which share 40% sequence identity. Nevertheless, our analysis demonstrates that some degree of rotational freedom exists in the RCC1-NCP complex and that the motion revolves around an anchoring attachment mediated through residue R217.

Other interactions found in the NCP-RCC1 crystal structure include RCC1's DNA-binding loop and N-terminal tail, both of which contact the nucleosomal DNA (Figure 5A). The positively charged, 41-residue N-terminal tail in *Drosophila* RCC1 (35 residues in the human protein) is partially resolved in the cryo-EM structure and was found to be required for stable nucleosome binding.[55] Both the DNA-binding loop and N-terminal tail have worse local resolution in the cryo-EM map compared with the rest of RCC1, with the N-terminal tail also only partially resolved. To explore potential dynamics in these regions, we performed 3DVA with a mask that included only the RCC1. Results from the first two principal components are included in Supplementary Movies 4−6 with their first and last frames presented in Figure 6. Component 0 shows a back-and-forth rocking motion of RCC1 parallel to the plane of the nucleosome, similar to component 0 of 3DVA with a mask that includes RCC1-Ran. This rocking motion gives rise to a dynamic interaction between the DNA-binding loop of RCC1 and the nucleosomal DNA, where the DNA-binding loop is observed to form transient contacts with the phosphate backbone at superhelical location 5 (SHL 5, Figure 6 and Supplemental Movie S5). The next 3DVA component captures motions in both the DNA-binding loop and N-terminal tail, with the latter interacting with the phosphate backbone at SHL 6

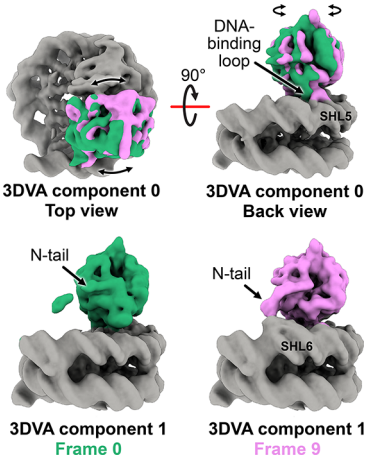

Figure 6. 3D variability analysis of the RCC1 region in the NCP-RCC1-Ran complex. Results from the first two principal components are shown where the first and last frames from each movie (Supplementary Movies 4−6) are colored green and pink, respectively. Curved arrows in the top half of the figure highlight the rocking motion detected in component 0. The DNA-binding loop and N-terminal tail of RCC1 are shown to contact the nucleosomal DNA at superhelical locations 5 (SHL5) and 6 (SHL6), respectively.

(Figure 6 and Supplemental Movie S6), one groove adjacent to the contact site of the DNA-binding loop.

The 3DVA analysis described above illustrates that RCC1 forms multiple interactions with nucleosomal DNA in the NCP-RCC1-Ran complex, consistent with previous observations.[28,55]

https://doi.org/10.1021/acs.biochem.3c00724
Biochemistry 2024, 63, 880−892

DNA binding contributes to the stability of the complex, with the dynamic nature of the NCP-RCC1 interactions contributing to the rapid on/off rates of RCC1 from chromatin.[56] RCC1 dissociation/reassociation is further influenced by posttranslational modifications and by dynamic interactions between RCC1, Ran, and other regulators such as importin α/β and RanBP1.[57−60] For example, increased phosphorylation of the RCC1 N-terminal tail at serine 2 and serine 11 during mitosis displaces RCC1 from the soluble importin α/β pool, promoting RCC1 binding to chromatin and cell cycle progression.[58,61,62] Although α-methylation of RCC1's N-terminal serine or proline by N-terminal methyl transferase 1 (after removal of the initiating methionine; note that human RCC1 has serine, other species often have proline) is not known to be regulated during the cell cycle, this posttranslational modification also enhances RCC1 association with chromatin in cells.[63−65] The NCP-RCC1 interaction can be further controlled by the presence of three different RCC1 splicing isoforms in mammalian cells.[66] While our study employed the canonical α-isoform, RCC1β and RCC1γ feature longer N-terminal tails that differ in their propensities for posttranslational modification and their affinities for chromatin compared to RCC1α.[66] Thus, the dynamics of RCC1 in the context of chromatin can be modulated in a variety of ways.

Ran Nucleotide-Binding Site in the NCP-RCC1-Ran Complex Resembles a GDP-Bound Pocket. Given that, in the structure presented here, Ran is in complex with RCC1 and the sample was treated with apyrase prior to grid freezing (the GTPase-GEF complex has higher affinity in the absence of nucleotide[44,45]), we expected that Ran would be nucleotide free. The overall architecture of Ran in our NCP-RCC1-Ran complex, including the conformations of switch regions and the C-terminal tail, closely resembles the previously determined RCC1-Ran•apo crystal structure (Figure 3D).[49] However, the nucleotide-binding pocket of Ran in the cryo-EM map resembles the conformation seen with GDP-bound Ran (Figure 7). In the crystal structure of Ran•GDP, the guanine base and ribose group of the bound GDP are sandwiched between a pair of lysine residues, K123 and K152 (Figure 7A).[49] An aspartate residue (D125) caps the binding pocket, forming hydrogen bonds with both the N1 imino and N2 amino groups of the guanine base. The α- and β-phosphate groups of GDP are stabilized by numerous electrostatic and hydrogen bonding interactions with the phosphate-binding loop (P-loop) of the GTPase. A Mg^{2+} ion sits below the β-phosphate and is coordinated with the hydroxyl group of T24, an oxygen atom from the β-phosphate, and four water molecules in an octahedral arrangement. In the RCC1-Ran•apo crystal structure, a reorganization of the nucleotide-binding pocket is observed (Figure 7B), with the side chains of K123, K152, and D125 reoriented because of conformational changes in loops capping the guanine base, disrupting key contacts with the nucleotide and leading to GDP release. The P-loop is unchanged from the GDP-bound structure, interacting with a crystallographic sulfate ion in place of β-phosphate in GDP.

In contrast to the RCC1-Ran•apo crystal structure, the nucleotide-binding site is preserved in the cryo-EM map of the NCP-RCC1-Ran complex, although it is less well formed than that in the Ran•GDP crystal structure (Figure 7C,D). Residues K123, K152, and D125 are in conformations similarly to what is observed in the Ran•GDP structure, with K123 in both crystallographic and cryo-EM-determined models largely overlapping. The portion of the loop following D125 is unresolved in the cryo-EM structure, indicating dynamics or heterogeneity in this region of the nucleotide pocket. In addition, density is observed where the guanine base of GDP would normally be found (Figure 7C, dotted oval). This density may derive from unresolved loops that would normally interact with the guanine base or from guanosine monophosphate (GMP), the product of GDP hydrolysis by apyrase that could have some affinity for Ran. It is also possible that the apyrase treatment was incomplete, leading to a small remaining amount of GDP in the sample upon grid freezing and resulting in partial occupancy of the nucleotide-binding pocket. Attempts to classify the data set into apo and ligand-bound classes were unsuccessful. Although complexes of nucleotide-bound G proteins and their constituent

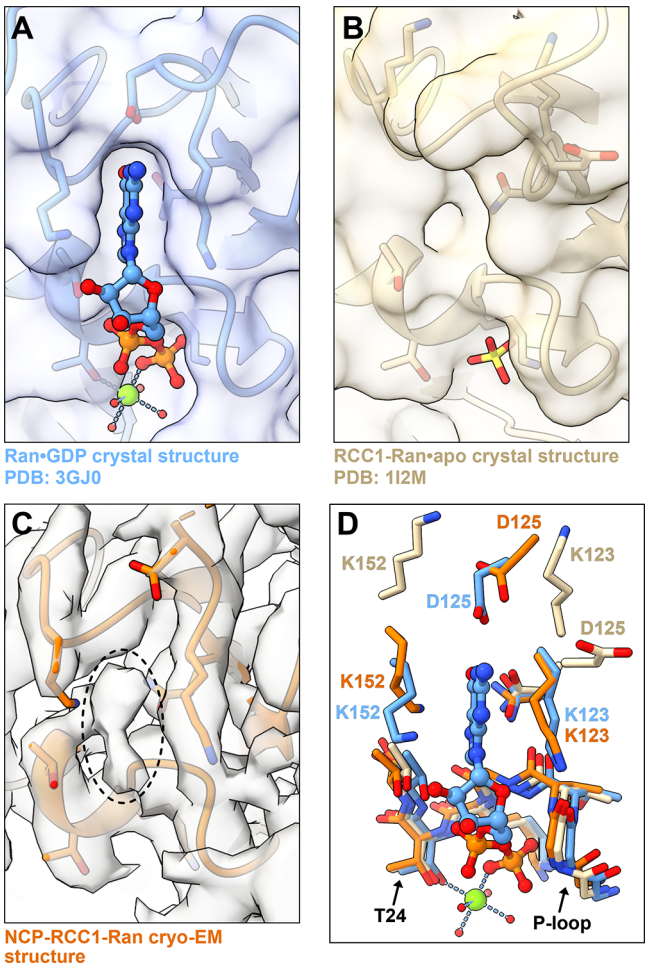

Figure 7. Nucleotide-binding pocket is largely preserved in the NCP-RCC1-Ran cryo-EM structure. Comparison of Ran's nucleotide-binding pocket between the Ran•GDP crystal structure (A, PDB: 3GJ0[49]), the nucleotide-free RCC1-Ran crystal structure (B, PDB: 1I2M[27]), and the NCP-RCC1-Ran cryo-EM structure (C). In panels A and B, the nucleotide pocket is depicted in both cartoon and solvent-accessible surface representation, with key residues shown as sticks. In panel C, the cryo-EM map is shown, along with the fitted atomic model. An unidentified density (dotted oval) is found in place of the GDP. (D) An overlay of the structures from panels A−C highlighting residues that play a role in GDP binding. The Ran•GDP crystal structure is colored blue, the nucleotide-free RCC1-Ran crystal structure is colored wheat, and the NCP-RCC1-Ran cryo-EM structure is colored orange. In panels A and D, GDP is depicted in ball and stick, while Mg^{2+} and the chelating water molecules are depicted as green and red spheres, respectively. In panel B, a crystallographic sulfate anion is depicted in sticks.

https://doi.org/10.1021/acs.biochem.3c00724
Biochemistry 2024, 63, 880−892

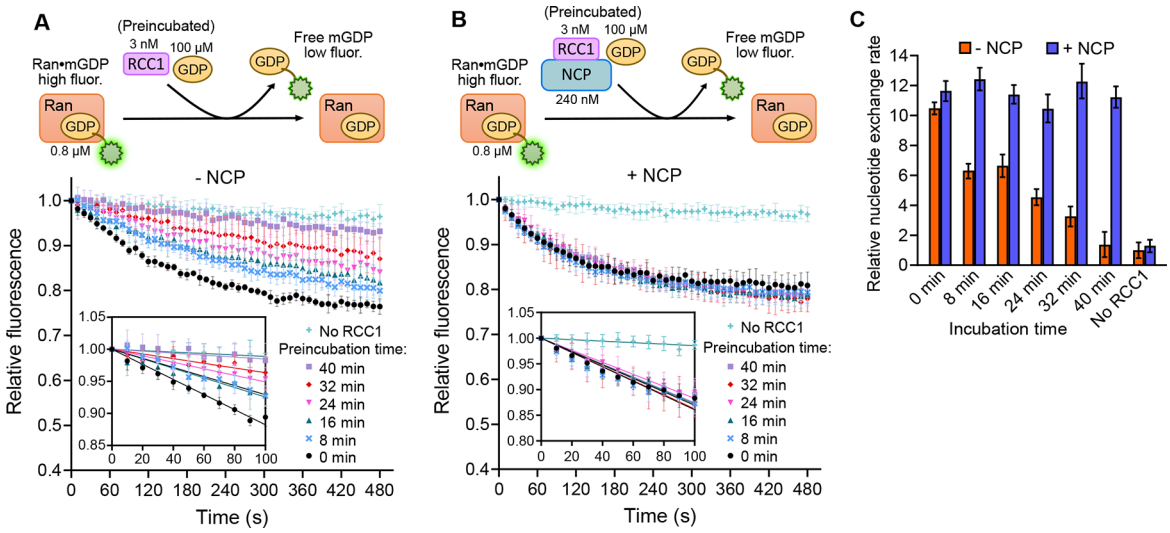

Figure 8. NCP stabilizes purified RCC1 *in vitro*. (A, B) Top: MANT-GDP exchange assay. A decrease in MANT fluorescence is observed when Ran-bound MANT-GDP (Ran•mGDP) is displaced by unlabeled GDP. Bottom: plots of fluorescence vs time after the injection of unlabeled GDP (100 μM final concentration) and RCC1 (3 nM final concentration) in the absence (A) or presence (B) of NCP (240 nM final concentration) to a starting solution of Ran-MANT-GDP. Prior to injection, flash-frozen aliquots of RCC1 were thawed and preincubated in buffer containing unlabeled GDP either without (A) or with (B) NCP for the indicated time (legend). Insets show the first 100 s of the MANT-GDP dissociation curves where least-squares linear regression was carried out to calculate rates of nucleotide exchange. Data points show the mean, and error bars indicate ± the standard deviation (n = 4 independent assays), with linear regression performed while treating each replicate value as an individual point. (C) Relative nucleotide exchange rates, calculated by taking the ratio of the slope for each fitted line from panels A and B to that in the absence of RCC1 and NCP (slope of the light blue line, no RCC1 in panel A). Error bars represent 95% confidence intervals in the ratios of slopes.

GEFs are generally transient,[44,45] RCC1-Ran-nucleotide complexes have been observed previously by fluorescence and NMR spectroscopy.[67,68] A final possibility is that, although the overall architecture of the NCP-RCC1-Ran complex resembles that of the RCC1-Ran•apo crystal structure, the presence of the NCP may stabilize a conformation of Ran•apo that retains a largely intact GDP-binding pocket.

NCP Stabilizes Purified RCC1 *In Vitro*. An early study found that the GEF activity of RCC1 is enhanced in the presence of nucleosomes.[24] In that study, both intact and trypsinized nucleosomes stimulated the RCC1-mediated GDP release in Ran by approximately 2-fold. Enhancement was also observed in the presence of histones H2A/H2B but not H3/H4, DNA, or a positively charged control protein, indicating that the effect was H2A/H2B- or nucleosome-specific. These observations suggest that nucleosomes serve at least as scaffolds to concentrate RCC1 and Ran on chromatin, thereby increasing the rate of nucleotide exchange. In addition, the nucleosome may also participate (either directly or allosterically) in the exchange process to accelerate the production of Ran•GTP, further contributing to the Ran•GTP gradient across the cell. To evaluate the role of chromatin in nucleotide exchange, we performed nucleotide exchange assays using 2′/3′-*O*-(*N*-methyl-anthraniloyl)-GDP (MANT-GDP), a fluorescent GDP analog (Figure 8). G-protein-bound MANT-GDP has a fluorescence intensity higher than that of the free fluorophore. Thus, in the presence of a GEF and an excess of unlabeled GDP, a decrease in fluorescence intensity from G-protein-bound MANT-GDP is observed over time, as MANT-GDP is replaced by unlabeled GDP. To compare RCC1-mediated nucleotide exchange in Ran with and without NCPs, reactions were initiated by injecting a stock solution containing RCC1 and unlabeled GDP into a starting solution of Ran preloaded with MANT-GDP. Prior to injection, RCC1/GDP stocks were preincubated either alone or with excess NCP (relative to RCC1). In both cases, a decrease in fluorescence was observed upon addition of the RCC1/GDP mix, indicating the exchange of MANT-GDP in Ran with unlabeled GDP (Figure 8A,B). In the absence of NCPs, purified RCC1 appears to lose activity over time, as shown by slower rates of the fluorescence decrease when the preincubation period is lengthened (Figure 8A,C). In contrast, RCC1 activity is preserved in the presence of NCPs, with no observable changes to the fluorescence decay curves across the range of preincubation times (Figure 8B,C). This observation suggests that formation of the NCP-RCC1 complex is fast under our experimental conditions (80:1 NCP:RCC1) and that the lack of enhancement in the observed nucleotide exchange rate with the addition of NCPs (Figure 8C, 0 min incubation time) is not the result of incomplete equilibration of the reaction components. Instead, NCPs appear to have a stabilizing effect on RCC1, at least under our experimental conditions, preventing activity loss over time. It is conceivable that stabilization of RCC1 by chromatin (against misfolding or degradation) also occurs in cells, providing another layer of control for the Ran system.

CONCLUSIONS

The NCP-RCC1-Ran complex plays a critical role in maintaining cellular Ran•GTP gradients that drive a variety of biological processes.[69] Here, we determined the cryo-EM structures of this ternary complex. Our studies suggest that the NCP serves as a hub that concentrates RCC1 and Ran at its surface, with R217 of RCC1 providing a strong electrostatic anchor at the H2A/H2B acidic patch of the nucleosome and with the RCC1 DNA-binding loop and N-terminal tail interacting dynamically with nucleosomal DNA. Notably, regions of Ran are also dynamic in the complex. Ran's switch 1 region appears to transition between disordered and ordered conformations upon interaction with the αC helix of histone H2B, a process that may be important for stabilizing the complex. Our results further suggest that the nucleosome

https://doi.org/10.1021/acs.biochem.3c00724
Biochemistry 2024, 63, 880−892

scaffold plays a role in stabilizing RCC1, but has little effect, at least under our experimental conditions, on either directly or allosterically regulating GDP release and subsequent GTP binding in Ran.

■ ASSOCIATED CONTENT

Data Availability Statement

The electron cryomicroscopy map and associated model described in this article have been deposited in the Electron Microscopy Data Bank (EMDB) with accession codes EMD-42685, EMD-42834, EMD-42836, and the Protein Data Bank (PDB) with accession code 8UX1.

Supporting Information

The Supporting Information is available free of charge at https://pubs.acs.org/doi/10.1021/acs.biochem.3c00724.

Figures illustrating the image processing pipeline, micrographs and 2D classes, and Fourier shell correlation (FSC) curves for the 1-side bound NCP-RCC1-Ran map and the locally refined RCC1-Ran map (PDF)

(Movie S1) 3DVA component 0 for the RCC1-Ran region of the NCP-RCC1-Ran complex (MP4)

(Movie S2) 3DVA component 1 for the RCC1-Ran region of the NCP-RCC1-Ran complex (MP4)

(Movie S3) 3DVA component 2 for the RCC1-Ran region of the NCP-RCC1-Ran complex (MP4)

(Movie S4) Top view of 3DVA component 0 for the RCC1 region of the NCP-RCC1-Ran complex (MP4)

(Movie S5) Back view of 3DVA component 0 for the RCC1 region of the NCP-RCC1-Ran complex (MP4)

(Movie S6) 3DVA component 1 for the RCC1 region of the NCP-RCC1-Ran complex (MP4)

■ AUTHOR INFORMATION

Corresponding Authors

Shuya Kate Huang − *Department of Molecular Genetics, University of Toronto, Toronto, ON M5S 1A8, Canada; Department of Biochemistry and Department of Chemistry, University of Toronto, Toronto, ON M5S 1A8, Canada; Hospital for Sick Children, Program in Molecular Medicine, Toronto, ON M5G 1X8, Canada*; Email: sk.huang@mail.utoronto.ca

John L. Rubinstein − *Department of Biochemistry, University of Toronto, Toronto, ON M5S 1A8, Canada; Hospital for Sick Children, Program in Molecular Medicine, Toronto, ON M5G 1X8, Canada; Department of Medical Biophysics, University of Toronto, Toronto, ON M5G 1L7, Canada*; orcid.org/0000-0003-0566-2209; Email: john.rubinstein@utoronto.ca

Lewis E. Kay − *Department of Molecular Genetics, University of Toronto, Toronto, ON M5S 1A8, Canada; Department of Biochemistry and Department of Chemistry, University of Toronto, Toronto, ON M5S 1A8, Canada; Hospital for Sick Children, Program in Molecular Medicine, Toronto, ON M5G 1X8, Canada*; orcid.org/0000-0002-4054-4083; Email: lewis.kay@utoronto.ca

Complete contact information is available at: https://pubs.acs.org/10.1021/acs.biochem.3c00724

Notes

The authors declare no competing financial interest.

■ ACKNOWLEDGMENTS

S.K.H. acknowledges a postdoctoral fellowship from the Canadian Institutes of Health Research (CIHR). This work was supported by grants to L.E.K. from the Natural Sciences and Engineering Research Council of Canada (2015-04347) and from the CIHR (FND-50357). Enzyme assays relied on the infrastructure from The Hospital for Sick Children's Structural & Biophysical Core Facility. Cryo-EM data were collected at the Toronto High-Resolution High-Throughput cryo-EM facility supported by the Canada Foundation for Innovation and Ontario Research Fund.

■ REFERENCES

(1) Drivas, G. T.; Shih, A.; Coutavas, E.; Rush, M. G.; D'Eustachio, P. Characterization of Four Novel ras-Like Genes Expressed in a Human Teratocarcinoma Cell Line. *Mol. Cell. Biol.* **1990**, *10*, 1793−1798.

(2) Bischoff, F. R.; Ponstingl, H. Catalysis of guanine nucleotide exchange on Ran by the mitotic regulator RCC1. *Nature* **1991**, *354*, 80−82.

(3) Kalab, P.; Weis, K.; Heald, R. Visualization of a Ran-GTP Gradient in Interphase and Mitotic Xenopus Egg Extracts. *Science* **2002**, *295* (5564), 2452−2456.

(4) Izaurralde, E.; Kutay, U.; von Kobbe, C.; Mattaj, I. W.; Görlich, D. The asymmetric distribution of the constituents of the Ran system is essential for transport into and out of the nucleus. *EMBO J.* **1997**, *16*, 6535−6547.

(5) Görlich, D.; Panté, N.; Kutay, U.; Aebi, U.; Bischoff, F. R. Identification of different roles for RanGDP and RanGTP in nuclear protein import. *EMBO J.* **1996**, *15*, 5584−5594.

(6) Rexach, M.; Blobel, G. Protein Import into Nuclei: Association and Dissociation Reactions Involving Transport Substrate, Transport Factors, and Nucleoporins. *Cell* **1995**, *83*, 683−692.

(7) Moore, M. S.; Blobel, G. The GTP-binding protein Ran/TC4 is required for protein import into the nucleus. *Nature* **1993**, *365*, 661−663.

(8) Moroianu, J.; Blobel, G. Protein export from the nucleus requires the GTPase Ran and GTP hydrolysis. *Proc. Natl. Acad. Sci. U. S. A.* **1995**, *92*, 4318−4322.

(9) Kuersten, S.; Ohno, M.; Mattaj, I. W. Nucleocytoplasmic transport: Ran, beta and beyond. *Trends Cell Biol.* **2001**, *11*, 497−503.

(10) Carazo-Salas, R. E.; Guarguaglini, G.; Gruss, O. J.; Segref, A.; Karsenti, E.; Mattaj, L. W. Generation of GTP-bound Ran by RCC1 is required for chromatin-induced mitotic spindle formation. *Nature* **1999**, *400*, 178−181.

(11) Ohba, T.; Nakamura, M.; Nishitani, H.; Nishimoto, T. Self-Organization of Microtubule Asters Induced in Xenopus Egg Extracts by GTP-Bound Ran. *Science* **1999**, *284* (5418), 1356−1358.

(12) Hetzer, M.; Bilbao-Cortés, D.; Walther, T. C.; Gruss, O. J.; Mattaj, I. W. GTP Hydrolysis by Ran is Required for Nuclear Envelope Assembly. *Mol. Cell* **2000**, *5*, 1013−1024.

(13) Zhang, C.; Clarke, P. R. Chromatin-independent nuclear envelope assembly induced by Ran GTPase in Xenopus egg extracts. *Science* **2000**, *288* (5470), 1429−1432.

(14) Moore, W. J.; Zhang, C.; Clarke, P. R. Targeting of RCC1 to Chromosomes Is Required for Proper Mitotic Spindle Assembly in Human Cells. *Curr. Biol.* **2002**, *12*, 1442−1447.

(15) Budhu, A. S.; Wang, X. W. Loading and Unloading: Orchestrating Centrosome Duplication and Spindle Assembly by Ran/Crm1. *Cell cycle* **2005**, *4*, 1510.

(16) Wong, C. H.; Chan, H.; Ho, C. Y.; Lai, S. K.; Chan, K. S.; Koh, C. G.; Li, H. Y. Apoptotic histone modification inhibits nuclear transport by regulating RCC1. *Nat. Cell Biol.* **2009**, *11*, 36−45.

(17) Boudhraa, Z.; Carmona, E.; Provencher, D.; Mes-Masson, A. M. Ran GTPase: A Key Player in Tumor Progression and Metastasis. *Front. Cell Dev. Biol.* **2020**, *8*, 345.

(18) Klebe, C.; Wittinghofer, A.; Bischoff, F. R.; Ponstingl, H. Interaction of the Nuclear GTP-Binding Protein Ran with Its

Regulatory Proteins RCC1 and RanGAP1. *Biochemistry* **1995**, *34*, 639−647.
(19) Mahajan, R.; Delphin, C.; Guan, T.; Gerace, L.; Melchior, F. A small ubiquitin-related polypeptide involved in targeting RanGAP1 to nuclear pore complex protein RanBP2. *Cell* **1997**, *88*, 97−107.
(20) Hopper, A. K.; Traglia, H. M.; Dunst, R. W. The Yeast RNA1 Gene Product Necessary for RNA Processing Is Located in the Cytosol and Apparently Excluded From the Nucleus. *J. Cell Biol.* **1990**, *111*, 309−321.
(21) Seki, T.; Hayashi, N.; Nishimoto, T. RCCl in the Ran Pathway. *J. Biochem* **1996**, *120*, 207−214.
(22) Klebe, C.; Nishimoto, T.; Wittinghofer, F. Functional Expression in Escherichia coli of the Mitotic Regulator Proteins p24ran and p45rcc1 and Fluorescence Measurements of Their Interaction. *Biochemistry* **1993**, *32*, 11923−11928.
(23) Luger, K.; Mäder, A. W.; Richmond, R. K.; Sargent, D. F.; Richmond, T. J. Crystal structure of the nucleosome core particle at 2.8 Å resolution. *Nature* **1997**, *389*, 251−260.
(24) Nemergut, M. E.; Mizzen, C. A.; Stukenberg, T.; Allis, C. D.; Macara, I. G. Chromatin docking and exchange activity enhancement of RCC1 by histones H2A and H2B. *Science* **2001**, *292* (5521), 1540−1543.
(25) Fasci, D.; Van Ingen, H.; Scheltema, R. A.; Heck, A. J. R. Histone Interaction Landscapes Visualized by Crosslinking Mass Spectrometry in Intact Cell Nuclei. *Mol. Cell. Proteomics* **2018**, *17*, 2018−2033.
(26) Bilbao-Cortés, D.; Hetzer, M.; Längst, G.; Becker, P. B.; Mattaj, I. W. Ran Binds to Chromatin by Two Distinct Mechanisms. *Curr. Biol.* **2002**, *12*, 1151−1156.
(27) Renault, L.; Kuhlmann, J.; Henkel, A.; Wittinghofer, A. Structural Basis for Guanine Nucleotide Exchange on Ran by the Regulator of Chromosome Condensation (RCC1). *Cell* **2001**, *105*, 245−255.
(28) Makde, R. D.; England, J. R.; Yennawar, H. P.; Tan, S. Structure of RCC1 chromatin factor bound to the nucleosome core particle. *Nature* **2010**, *467*, 562.
(29) Abramov, G.; Velyvis, A.; Rennella, E.; Wong, L. E.; Kay, L. E. A methyl-TROSY approach for NMR studies of high-molecular-weight DNA with application to the nucleosome core particle. *Proc. Natl. Acad. Sci. U. S. A.* **2020**, *117*, 12836−12846.
(30) Kim, T. H.; Nosella, M. L.; Bolik-Coulon, N.; Harkness, R. W.; Huang, S. K.; Kay, L. E. Correlating histone acetylation with nucleosome core particle dynamics and function. *Proc. Natl. Acad. Sci. U. S. A.* **2023**, *120*, No. e2301063120.
(31) Marr, C. R.; Benlekbir, S.; Rubinstein, J. L. Fabrication of carbon films with ∼ 500 nm holes for cryo-EM with a direct detector device. *J. Struct. Biol.* **2014**, *185*, 42−47.
(32) Punjani, A.; Rubinstein, J. L.; Fleet, D. J.; Brubaker, M. A. CryoSPARC: Algorithms for rapid unsupervised cryo-EM structure determination. *Nat. Methods* **2017**, *14*, 290−296.
(33) Punjani, A.; Zhang, H.; Fleet, D. J. Non-uniform refinement: adaptive regularization improves single-particle cryo-EM reconstruction. *Nat. Methods* **2020**, *17*, 1214−1221.
(34) Ramírez-Aportela, E.; Vilas, J. L.; Glukhova, A.; Melero, R.; Conesa, P.; Martínez, M.; Maluenda, D.; Mota, J.; Jiménez, A.; Vargas, J.; Marabini, R.; Sexton, P. M.; Carazo, J. M.; Sorzano, C. O. S. Automatic local resolution-based sharpening of cryo-EM maps. *Bioinformatics* **2020**, *36*, 765−772.
(35) Martínez, M.; Jiménez-Moreno, A.; Maluenda, D.; Ramírez-Aportela, E.; Melero, R.; Cuervo, A.; Conesa, P.; Del Caño, L.; Fonseca, Y. C.; Sánchez-García, R.; Strelak, D.; Conesa, J. J.; Fernández-Giménez, E.; De Isidro, F.; Sorzano, C. O. S.; Carazo, J. M.; Marabini, R. Integration of Cryo-EM Model Building Software in Scipion. *J. Chem. Inf. Model.* **2020**, *60*, 2533−2540.
(36) Meng, E. C.; Goddard, T. D.; Pettersen, E. F.; Couch, G. S.; Pearson, Z. J.; Morris, J. H.; Ferrin, T. E. UCSF ChimeraX: Tools for structure building and analysis. *Protein Sci.* **2023**, *32*, No. e4792.
(37) Davey, C. A.; Sargent, D. F.; Luger, K.; Maeder, A. W.; Richmond, T. J. Solvent Mediated Interactions in the Structure of the Nucleosome Core Particle at 1.9 Å Resolution. *J. Mol. Biol.* **2002**, *319*, 1097−1113.
(38) Jumper, J.; Evans, R.; Pritzel, A.; Green, T.; Figurnov, M.; Ronneberger, O.; Tunyasuvunakool, K.; Bates, R.; Žídek, A.; Potapenko, A.; Bridgland, A.; Meyer, C.; Kohl, S. A. A.; Ballard, A. J.; Cowie, A.; Romera-Paredes, B.; Nikolov, S.; Jain, R.; Adler, J.; Back, T.; Petersen, S.; Reiman, D.; Clancy, E.; Zielinski, M.; Steinegger, M.; Pacholska, M.; Berghammer, T.; Bodenstein, S.; Silver, D.; Vinyals, O.; Senior, A. W.; Kavukcuoglu, K.; Kohli, P.; Hassabis, D. Highly accurate protein structure prediction with AlphaFold. *Nature* **2021**, *596* (7873), 583−589.
(39) Emsley, P.; Cowtan, K. Coot: model-building tools for molecular graphics. *Acta Crystallogr. Sect. D* **2004**, *60*, 2126−2132.
(40) Croll, T. I. ISOLDE: a physically realistic environment for model building into low-resolution electron-density maps. *Acta Crystallogr. Sect. D* **2018**, *74*, 519−530.
(41) Liebschner, D.; Afonine, P. V.; Baker, M. L.; Bunkoczi, G.; Chen, V. B.; Croll, T. I.; Hintze, B.; Hung, L. W.; Jain, S.; McCoy, A. J.; Moriarty, N. W.; Oeffner, R. D.; Poon, B. K.; Prisant, M. G.; Read, R. J.; Richardson, J. S.; Richardson, D. C.; Sammito, M. D.; Sobolev, O. V.; Stockwell, D. H.; Terwilliger, T. C.; Urzhumtsev, A. G.; Videau, L. L.; Williams, C. J.; Adams, P. D. Macromolecular structure determination using X-rays, neutrons and electrons: recent developments in Phenix. *Acta Crystallogr. Sect. D* **2019**, *75*, 861−877.
(42) Lowary, P. T.; Widom, J. New DNA sequence rules for high affinity binding to histone octamer and sequence-directed nucleosome positioning. *J. Mol. Biol.* **1998**, *276*, 19−42.
(43) Draizen, E. J.; Shaytan, A. K.; Mariño-Ramírez, L.; Talbert, P. B.; Landsman, D.; Panchenko, A. R. HistoneDB 2.0: a histone database with variants-an integrated resource to explore histones and their variants. *Database* **2016**, baw14.
(44) Bos, J. L.; Rehmann, H.; Wittinghofer, A. GEFs and GAPs: Critical Elements in the Control of Small G Proteins. *Cell* **2007**, *129*, 865−877.
(45) Lenzen, C.; Cool, R. H.; Prinz, H.; Kuhlmann, J.; Wittinghofer, A. Kinetic analysis by fluorescence of the interaction between Ras and the catalytic domain of the guanine nucleotide exchange factor Cdc25-(Mm). *Biochemistry* **1998**, *37*, 7420−7430.
(46) England, J. R.; Huang, J.; Jennings, M. J.; Makde, R. D.; Tan, S. RCC1 Uses a Conformationally Diverse Loop Region to Interact with the Nucleosome: A Model for the RCC1-Nucleosome Complex. *J. Mol. Biol.* **2010**, *398*, 518−529.
(47) McGinty, R. K.; Tan, S. Principles of nucleosome recognition by chromatin factors and enzymes. *Curr. Opin. Struct. Biol.* **2021**, *71*, 16−26.
(48) Skrajna, A.; Goldfarb, D.; Kedziora, K. M.; Cousins, E. M.; Grant, G. D.; Spangler, C. J.; Barbour, E. H.; Yan, X.; Hathaway, N. A.; Brown, N. G.; Cook, J. G.; Major, M. B.; McGinty, R. K. Comprehensive nucleosome interactome screen establishes fundamental principles of nucleosome binding. *Nucleic Acids Res.* **2020**, *48*, 9415−9432.
(49) Partridge, J. R.; Schwartz, T. U. Crystallographic and Biochemical Analysis of the Ran-binding Zinc Finger Domain. *J. Mol. Biol.* **2009**, *391*, 375−389.
(50) Wittinghofer, A.; Seewald, M. J.; Körner, C.; Vetter, I. R. RanGAP mediates GTP hydrolysis without an arginine finger. *Nature* **2002**, *415*, 662−666.
(51) Scheffzek, K.; Klebe, C.; Fritz-Wolf, K.; Kabsch, W.; Wittinghofer, A. Crystal structure of the nuclear Ras-related protein Ran in its GDP-bound form. *Nature* **1995**, *374*, 378−381.
(52) Punjani, A.; Fleet, D. J. 3D variability analysis: Resolving continuous flexibility and discrete heterogeneity from single particle cryo-EM. *J. Struct. Biol.* **2021**, *213*, No. 107702.
(53) Shaffer, J. M.; Jiou, J.; Tripathi, K.; Olaluwoye, O. S.; Fung, H. Y. J.; Chook, Y. M.; D'Arcy, S. Molecular basis of RanGTP-activated nucleosome assembly with Histones H2A-H2B bound to Importin-9. *bioRxiv* **2023**, 2023-01.
(54) Jiou, J.; Shaffer, J. M.; Bernades, N. E.; Fung, H. Y. J.; Kikumoto Dias, J.; D'Arcy, S.; Chook, Y. M. Mechanism of RanGTP priming H2A-H2B release from Kap114 in an atypical RanGTP●Kap114●H2A-H2B complex. *Proc. Natl. Acad. Sci. U. S. A.* **2023**, *120*, No. e2301199120.

https://doi.org/10.1021/acs.biochem.3c00724
Biochemistry 2024, 63, 880−892

(55) Hao, Y.; Macara, I. G. Regulation of chromatin binding by a conformational switch in the tail of the Ran exchange factor RCC1. *J. Cell Biol.* **2008**, *182*, 827−836.
(56) Li, H. Y.; Wirtz, D.; Zheng, Y. A mechanism of coupling RCC1 mobility to RanGTP production on the chromatin in vivo. *J. Cell Biol.* **2003**, *160*, 635−644.
(57) Cushman, I.; Stenoien, D.; Moore, M. S. The Dynamic Association of RCC1 with Chromatin Is Modulated by Ran-dependent Nuclear Transport. *Mol. Biol. Cell* **2004**, *15*, 245.
(58) Hutchins, J. R. A.; Moore, W. J.; Hood, F. E.; Wilson, J. S. J.; Andrews, P. D.; Swedlow, J. R.; Clarke, P. R. Phosphorylation Regulates the Dynamic Interaction of RCC1 with Chromosomes during Mitosis. *Curr. Biol.* **2004**, *14*, 1099−1104.
(59) Yau, K. C.; Arnaoutov, A.; Aksenova, V.; Kaufhold, R.; Chen, S.; Dasso, M. RanBP1 controls the Ran pathway in mammalian cells through regulation of mitotic RCC1 dynamics. *Cell Cycle* **2020**, *19*, 1899−1916.
(60) Zhang, M. S.; Arnaoutov, A.; Dasso, M. RanBP1 governs spindle assembly by defining mitotic Ran-GTP production. *Dev. Cell* **2014**, *31*, 393−404.
(61) Hou, X.; Qiao, L.; Liu, R.; Han, X.; Zhang, W. Phosphorylation of RCC1 on serine 11 facilitates G1/S transition in HPV E7-expressing cells. *MDPI Biomol.* **2021**, *11*, 995.
(62) Li, H. Y.; Zheng, Y. Phosphorylation of RCC1 in mitosis is essential for producing a high RanGTP concentration on chromosomes and for spindle assembly in mammalian cells. *Genes Dev.* **2004**, *18*, 512−527.
(63) Chen, T.; Muratore, T. L.; Schaner-Tooley, C. E.; Shabanowitz, J.; Hunt, D. F.; Macara, I. F. N-terminal α-methylation of RCC1 is necessary for stable chromatin association and normal mitosis. *Nat. Cell Biol.* **2007**, *9*, 596.
(64) Hitakomate, E.; Hood, F. E.; Sanderson, H. S.; Clarke, P. R. The methylated N-terminal tail of RCC1 is required for stabilisation of its interaction with chromatin by Ran in live cells. *BMC Cell Biol.* **2010**, *11*, 1−10.
(65) Schaner Tooley, C. E.; Petkowski, J. J.; Muratore-Schroeder, T. L.; Balsbaugh, J. L.; Shabanowitz, J.; Sabat, M.; Minor, W.; Hunt, D. F.; MacAra, I. G. NRMT is an α-N-methyltransferase that methylates RCC1 and Retinoblastoma Protein. *Nature* **2010**, *466*, 1125.
(66) Hood, F. E.; Clarke, P. R. RCC1 isoforms differ in their affinity for chromatin, molecular interactions and regulation by phosphorylation. *J. Cell Sci.* **2007**, *120*, 3436−3445.
(67) Klebe, C.; Prinz, H.; Wittinghofer, A.; Goody, R. S. The Kinetic Mechanism of Ran-Nucleotide Exchange Catalyzed by RCC1. *Biochemistry* **1995**, *34*, 12543−12552.
(68) Geyer, M.; Assheuer, R.; Klebe, C.; Kuhlmann, J.; Becker, J.; Wittinghofer, A.; Kalbitzer, H. R. Conformational states of the nuclear GTP-binding protein ran and its complexes with the exchange factor RCC1 and the effector protein RanBP1. *Biochemistry* **1999**, *38*, 11250−11260.
(69) Zierhut, C.; Funabiki, H. Nucleosome functions in spindle assembly and nuclear envelope formation. *BioEssays* **2015**, *37*, 1074−1085.

https://doi.org/10.1021/acs.biochem.3c00724
Biochemistry 2024, 63, 880−892